The ferroelectric nematic phase: on the role of lateral alkyloxy chains

Ewan Cruickshank, Abigail Pearson, Stevie Brown, John MD Storey, Corrie T Imrie & Rebecca Walker

Published online: 12 Jun 2023.

Submit your article to this journal

Article views: 852

View related articles

View Crossmark data

Taylor & Francis
Taylor & Francis Group

🔓 OPEN ACCESS | Check for updates

The ferroelectric nematic phase: on the role of lateral alkyloxy chains

Ewan Cruickshank ⓘD, Abigail Pearson, Stevie Brown, John MD Storey ⓘD, Corrie T Imrie ⓘD and Rebecca Walker ⓘD

Department of Chemistry, School of Natural and Computing Sciences, University of Aberdeen, Aberdeen, UK

ABSTRACT

The synthesis and characterisation of the 4-({[4′-nitro-(1,1′-biphenyl)−4-yl]oxy}carbonyl)phenyl 2-alkoxy-4-methoxybenzoates are reported: the 1O(m-On)PEPEBNO$_2$ series. These materials include an additional phenyl ring compared to the extensively studied ferroelectric nematogen RM734, added to increase the liquid crystal transition temperatures. All members of the series exhibited both conventional nematic (N) phase and ferroelectric nematic (N$_F$) phases; T$_{NI}$ and T$_{NFN}$ both decrease on increasing n, the length of the lateral alkoxy chain. The properties of this four-ring series are compared with analogous three-ring laterally substituted variants of RM734; the addition of the extra phenyl ring has a significantly more pronounced effect on the value of T$_{NI}$ than on T$_{NFN}$. The increase in T$_{NI}$ may be attributed to the enhanced structural anisotropy and more favourable intermolecular interactions arising from the insertion of the phenyl ring, whereas the much weaker effect on T$_{NFN}$ may reflect a change in the shape of the molecule. We also report two materials with three-ring structures, the 4′-nitro-(1,1′-biphenyl)-4-yl 2-alkoxy-4-methoxybenzoates: 1O(m-On)PEBNO$_2$ (n = 1 and 2). The removal of the ester linkage between RM734 and 1O(m-O1)PEPNO$_2$ extinguishes the N$_F$ phase and this appears to be consistent with a model in which the molecules are described in terms of a longitudinal surface charge density wave.
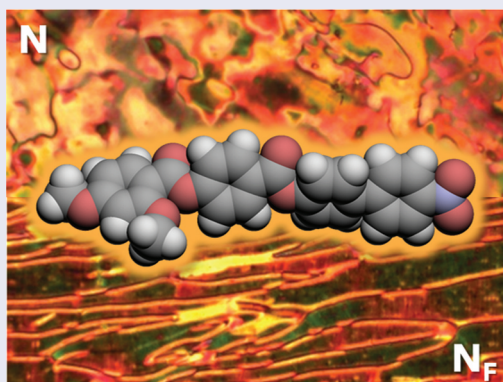
Introduction

The least ordered liquid crystal phase, the conventional nematic phase (N), is technologically the most significant, being used extensively in display devices [1]. In the N phase, the centres of mass of the rod-like molecules are arranged randomly, but their long axes are pointed along a common direction known as the director, represented by the unit vector **n**, Figure 1(a). The N phase has inversion symmetry (i.e. **n** = -**n**) and is therefore non-polar. Predictions of a polar nematic phase – one without inversion symmetry (**n** ≠ -**n**, Figure 1(b)) – were made first by Max Born in 1916, who suggested that

such a polar fluid would exist if its constituent molecules possessed sufficiently large dipole moments that dipole-dipole interactions between molecules could overcome thermal fluctuations [2]. Experimentally, however, such a phase was only observed over a century later. In 2017, independent and simultaneous reports described two materials – RM734 [3,4] and DIO [5], Figure 2 – that exhibited ferroelectric ordering in a nematic phase at temperatures below the conventional N phase [6]. This lower temperature nematic phase, later assigned as the ferroelectric nematic phase (N$_F$), shows a huge spontaneous polarisation and strong non-linear optical response [6,7]. These remarkable properties, coupled
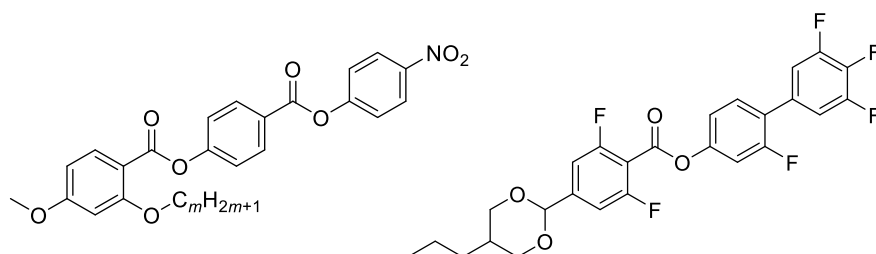

CONTACT Rebecca Walker ✉ rebecca.walker@abdn.ac.uk
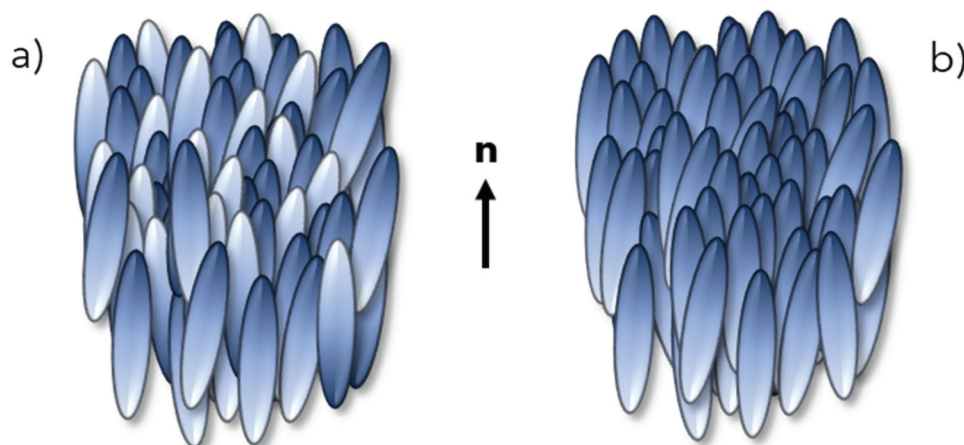
Figure 1. (Colour online) Sketches of (a) the conventional uniaxial nematic, N, and (b) the ferroelectric nematic, N_F, phases.


Figure 2. Molecular structures of (left) the **5**-*m* series (5–1 = RM734) and (right) DIO.

with nematic fluidity, are not only of huge fundamental significance but also endow the N_F phase with the very real potential to revolutionise liquid crystal–based technologies.

The rational design of materials capable of exhibiting the N_F phase requires an understanding of the relevant structure–property relationships and these empirical relationships have still to be established let alone understood. The archetypal ferroelectric nematogens, RM734 and DIO, both have large longitudinal molecular dipole moments and some degree of lateral steric bulk – either a lateral methoxy group or a large degree of fluorination, respectively – features that appear to be pre-requisites for the observation of the N_F phase. Relatively subtle structural changes to these molecules have yielded a range of materials that show ferroelectric nematic behaviour [8–17]. Most recently, a supramolecular hydrogen-bonded ferroelectric nematogen has been reported that has a much smaller longitudinal dipole moment than the covalently bonded examples [18]. This highlights the pressing need to enhance our understanding of the structural features required to observe the N_F phase and this can only be achieved through the synthesis and characterisation of new materials.

We recently reported the effect of lengthening the lateral alkoxy chain in two series of materials based on

RM734, **5**-*m* and **6**-*m*, the former is shown in Figure 2 [19]. This study revealed that the bulky lateral alkyloxy chain stabilises the N_F phase relative to the N phase, and here we seek to exploit this ability of the N_F phase to tolerate bulky lateral substituents and report the synthesis and characterisation of the 4-({[4'-nitro-(1,1'-biphenyl)-4-yl]oxy}carbonyl)phenyl 2-alkoxy–4-methoxybenzoates, Figure 3. These materials include an additional phenyl ring compared to RM734 in an attempt to increase the liquid crystal transition temperatures. The materials are referred to by the acronym 1O(m-O*n*)PEPEBNO$_2$, where 1O is the terminal methoxy group, P a phenyl ring, E an ester, B a biphenyl moiety and NO$_2$ the nitro terminal group. The bracketed part denotes the lateral alkyloxy chain, where *n* is the number of carbon atoms in the chain and m signifies that the lateral group is in the
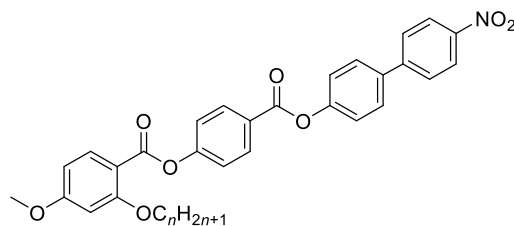
Figure 3. Structure of the 1O(m-O*n*)PEPEBNO$_2$ series, where *n* = 1–9.
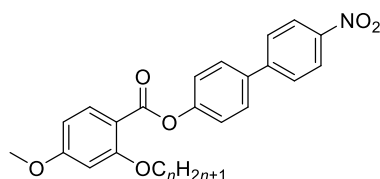
Figure 4. Structure of the 1O(m-O*n*)PEBNO$_2$ series, where *n* = 1–2.

meta position with respect to the terminal chain. The homologues with *n* = 1–9 have been studied, and their properties compared to those of the **5**-*m* series.

We also report two materials with three-ring structures, in which the central benzoate moiety has been removed: 4'-nitro-(1,1'-biphenyl)-4-yl 2,4-dimethoxybenzoate (1O(m-O1)PEBNO$_2$) and 4'-nitro-(1,1'-biphenyl)-4-yl 2-ethoxy-4-methoxybenzoate (1O(m-O2)PEBNO$_2$), Figure 4, and compare their properties to the corresponding members of the four-ring series and to the **5**-*m* series.

Experimental

Synthesis

The synthetic route used to prepare the 1O(m-O*n*)PEPEBNO$_2$ series is shown in Scheme 1 and the 1O(m-O*n*)PEBNO$_2$ series in Scheme 2. A detailed description of the preparation of all intermediates and final homologues along with structural characterisation data is provided in the Supplementary Information.

Optical studies

Phase characterisation was performed using polarised optical microscopy (POM), using an Olympus BH2
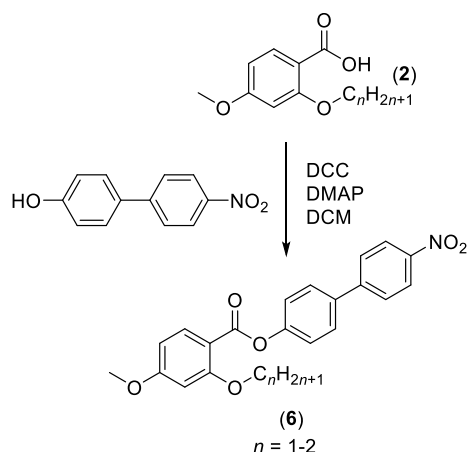
Scheme 2. Synthetic route used to prepare the 1O(m-O*n*)PEBNO$_2$ homologues, where *n* = 1–2.

polarising light microscope equipped with a Linkam TMS92 hot stage and a Zeiss AxioImager A2m equipped with a Linkam THMS600 hot stage. Planar aligned cells with an ITO conducting layer and a cell thickness of 2.9–3.5 μm were purchased from INSTEC.

Thermal studies

Thermal behaviour of the materials was studied using differential scanning calorimetry (DSC) using a Mettler Toledo DSC1 equipped with a TSO 801RO sample robot and calibrated using indium and zinc standards. Heating and cooling rates were 10°C min^{-1} in all cases, with a 3-min isotherm between heating and cooling segments. Thermal data were extracted from the second heating trace unless otherwise stated. Samples were run in
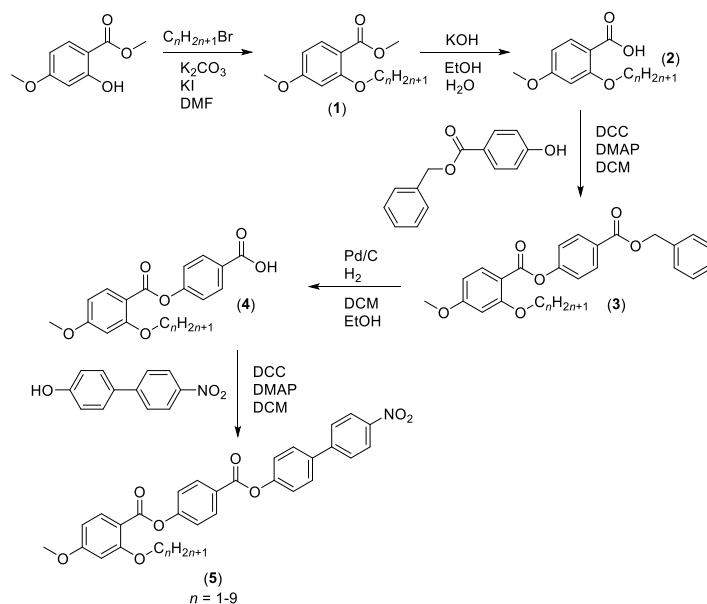
Scheme 1. Synthetic route used to prepare the 1O(m-O*n*)PEPEBNO$_2$ series, where *n* = 1–9.

duplicate and an average of the two measurements of temperature and entropy change is reported. The thermal stability of $1O(m\text{-}O1)PEPEBNO_2$ was evaluated using thermogravimetric analysis (TGA) using a Mettler Toledo TGA2 STAR^e system equipped with a small furnace (1100°C limit) and a sample robot.

Molecular modelling

The geometric parameters of the $1O(m\text{-}On)PEPEBNO_2$ series were obtained using quantum mechanical DFT calculations with Gaussian09 software [20]. Optimisation of the molecular structures was carried out at the B3LYP/6-31 G(d) level of theory. Visualisations of electronic surfaces were generated from the optimised geometries using GaussView5 software and visualisations of the space-filling models were produced post-optimisation using the QuteMol package [21].

Results & discussion

The transitional properties of the $1O(m\text{-}On)PEPEBNO_2$ series are listed in Table 1, and the dependence of the transition temperatures on the length of the lateral chain is shown in Figure 5. All the reported members of the series show N_F and N phases; the N phase is enantiotropic for homologues $n = 1\text{-}7$ and monotopic for $n = 8$ and 9. The homologue with $n = 1$ decomposes prior to clearing (seen in DSC and TGA traces, shown in Figure S1 and S2, respectively) and thus the value of T_{NI} reported for this is a low estimate. The ferroelectric nematic phase is strongly monotropic for all homologues i.e. T_{NFN} falls far below the melting point such that crystallisation precludes the observation of the transition using DSC (see Figure S3 for an example) and instead is only observed by extensive supercooling when viewed through a polarised optical microscope.

The N and N_F phases were assigned based on optical textures observed using POM. Specifically, N phases were assigned by observing either a characteristic
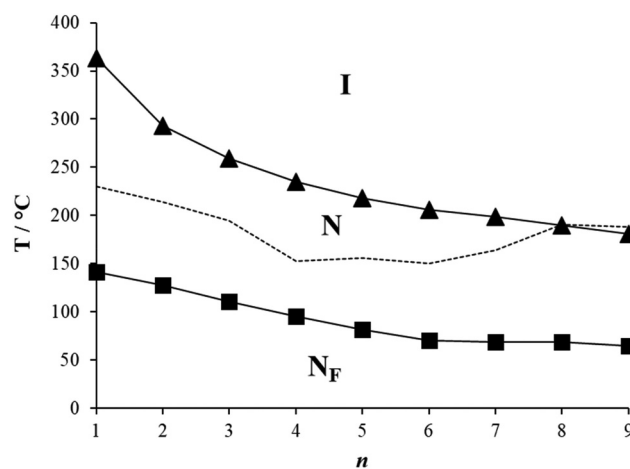
Table 1. Transition temperatures and associated scaled entropy changes for the $1O(m\text{-}On)PEPEBNO_2$ series.

n	T_{Cr}/°C	T_{NFN}/°C†	T_{NI}/°C	ΔS_{Cr}/R	ΔS_{NI}/R
1	230	(141)	[a]363	14.4	-
2	214	(128)	293	15.3	0.20
3	195	(111)	259	14.0	0.15
4	153	(95)	235	15.7	0.13
5	156	(82)	218	18.6	0.11
6	150	(70)	206	12.8	0.10
7	164	(69)	199	14.6	0.10
8	191	(69)	(190)	17.4	0.09
9	188	(65)	(181)	17.0	0.09

†temperatures obtained using POM.
[a]sample decomposes prior to clearing, temperature obtained using TGA.
() denotes a monotropic transition.

Figure 5. Dependence of the transition temperatures on the number of carbon atoms in the lateral alkyloxy chain, n, for the $1O(m\text{-}On)PEPEBNO_2$ series. Values of T_{NI} are represented by triangles, T_{NFN} by squares and the melting points by the dashed line.

schlieren texture containing two- and four-point brush defects, which flashed when subjected to mechanical stress, or a uniform texture when viewed between untreated glass slides and in planar aligned cells, respectively. A representative texture is given in Figure 6(a). The scaled entropy changes associated with the nematic–isotropic transition are consistent with this assignment. The value of $\Delta S_{NI}/R$ decreases on increasing n and this may reflect the increasing biaxiality of the compounds as the length of the lateral chain is extended [22,23].

Cooling the N phase saw a striking change in birefringence and the emergence of domain boundaries, see Figure 6(b). The orientation of the director differs between the domains and thus has different polarisations. The formation of these domains is thought to be driven by director splay deformations and is required to connect the opposite polarisation vectors on the lower and upper cell surfaces [8]. This texture has been termed a 'banded' texture and is thought to be characteristic of the N_F phase [11,19]. The highly monotropic nature of the N_F phase precluded its study using dielectric spectroscopy or second harmonic generation measurements, normally used to confirm the assignment of the N_F phase, due to rapid crystallisation of the sample nearly simultaneous with the N_F-N transition. To confirm our phase assignments, we have instead constructed binary-phase diagrams using mixtures of the well-characterised ferroelectric nematogen RM734 with two of our materials, homologues $n = 4$ and $n = 7$, and these are shown in Figure 7. Complete miscibility between the two components was observed over the whole composition range, confirming the N and N_F assignments. The textures observed were the same as those shown in Figure 6.
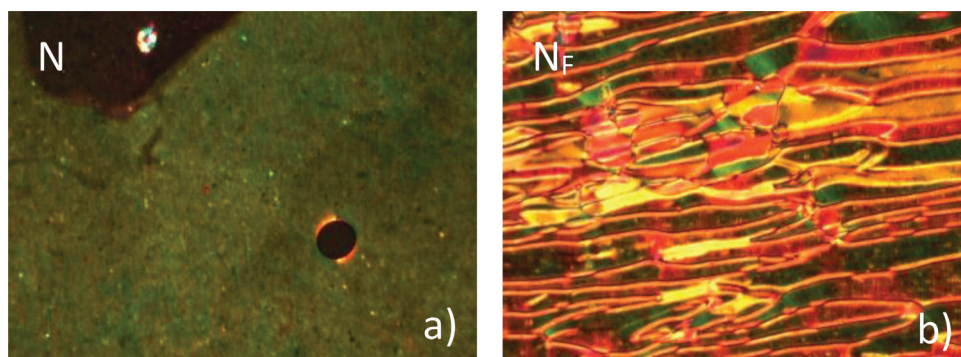
Figure 6. (Colour online) Textures of 1O(m-O3)PEPEBNO$_2$ in (a) the N phase at 116°C and (b) in the N$_F$ phase at 94°C in a planar aligned cell.

Figure 7. Phase diagrams constructed using binary mixtures of 1O(m-O4)PEPEBNO$_2$ (left) and 1O(m-O7)PEPEBNO$_2$ (right) with the archetypal ferroelectric nematogen RM734. Values of T$_{NI}$ are represented by triangles, T$_{NFN}$ by squares and the melting point by the dashed line.

The values of T$_{NI}$ increased as the concentration of RM734 decreased in both phase diagrams, whereas the values of T$_{NFN}$ showed a linear decrease on decreasing the concentration of RM734 in the mixtures. The virtual values of T$_{NFN}$ estimated from the phase diagrams for n = 4 and n = 7 were in excellent agreement with the temperatures found for the pure compounds using POM, providing further confirmation of these phase assignments.

The dependence of transition temperatures on the length of the lateral chain, n, for the 1O(m-On)PEPEBNO$_2$ series is shown in Figure 5. The shortest homologue, n = 1, has the highest value of T$_{NI}$ (although as noted in Table 1, this is accompanied by decomposition), and on increasing n, there is an initial sharp drop in T$_{NI}$ which lessens at values of $n \geq 3$ to a more gradual decrease. T$_{NFN}$ also decreases on increasing n; however, the values appear to reach to a limiting value in homologues with $n \geq 6$. The melting points do not appear to show a regular dependence on varying n.

The transition temperatures of the 1O(m-On)PEPEBNO$_2$ series are compared with those of the structurally similar **5**-m series, **Table S1**, in Figure 8 [9,19]. We note that **5**-1 is the extensively studied RM734, Figure 2. The replacement of the nitrophenyl group in **5**-m by a nitrobiphenyl moiety in the 1O(m-On)PEPEBNO$_2$ series has a substantial impact on T$_{NI}$ which increases, on average, by 155°C. This increase may be attributed to the enhanced intermolecular interactions between the mesogenic units, in addition to the greater shape anisotropy endowed by the additional phenyl ring, Figure 9. The values of T$_{NI}$ for both series decrease as the length of the lateral alkyloxy-chain increases and appears to converge towards or reach a limiting value. Similar behaviour was first reported for low molar mass mesogens containing a lateral alkyl chain by Weissflog and Demus [24,25] and was thought to imply that the lateral alkyl chain adopts conformations in which it lies parallel to the molecular axis, although such an assumption is not required to account for this behaviour [26].

The values of T$_{NFN}$ for the 1O(m-On)PEPEBNO$_2$ and **5**-m series are more similar and on average 24°C higher for the 1O(m-On)PEPEBNO$_2$ series than for the
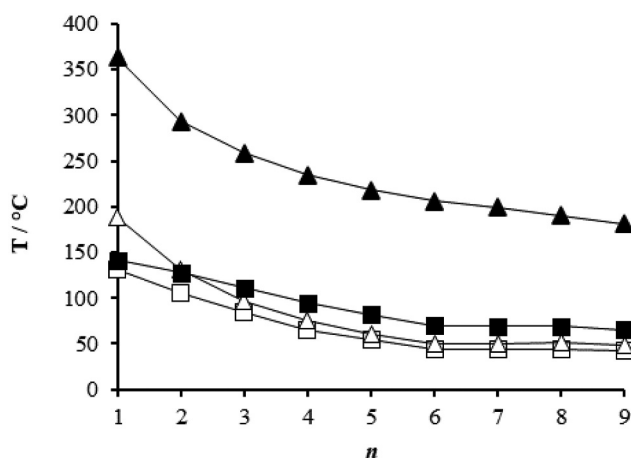
Figure 8. Dependence of the transition temperatures on the number of carbon atoms in the lateral alkyloxy chain, *n*, for the 1O(m-O*n*)PEPEBNO$_2$ series (filled symbols) and **5**-*m* series (open symbols). Values of T_{NI} are represented by triangles and T_{NFN} by squares.

corresponding member of the **5**-*m* series. Their dependence on the length of the lateral chain is very similar but weaker than that seen for T_{NI}. This may reflect that increasing the chain length inhibits the anti-parallel associations between the molecules and offsets the dilution factor associated with increasing the volume fraction of chains.

The question is how to account for this increase in the values of T_{NFN} on the insertion of the phenyl ring? We saw earlier that the longitudinal molecular dipole moment is thought to be important in driving the formation of the N_F phase, but this is just 0.31 D higher for 1O(m-O1)PEPEBNO$_2$ than for **5**-1 (RM734) – the dipole moments being 11.71 D and 11.40 D, respectively – and this would appear too modest an increase to account for the change in transition temperatures. The enhanced structural anisotropy resulting from the insertion of the phenyl ring changes the molecular shape of 1O(m-O1)PEPEBNO$_2$ and should not be thought of as simply increasing the length-to-breadth ratio compared to that of **5**-1. It may be that the increase in T_{NFN}

reflects this change in shape. Alternatively, Madhusudana has proposed a model in which the rod-like molecules in the N_F phase may be described as possessing longitudinal surface charge density waves and the interaction between these drives the formation of the N_F phase [27]. Within the framework of the model, the rod-like molecules are represented by regions of alternating positive and negative charges dictated by the electron-withdrawing or donating nature of the functional groups substituted onto the aromatic rings. One terminus of the rod is positively charged and the other negatively, giving a net longitudinal dipole moment. If these rods exist in close proximity, then the neighbouring molecules are sensitive to each other's charge distribution and preferentially pack in a parallel manner. Reducing the amplitude of the charge density wave at either end of the molecule enhances the parallel alignment of the molecules. The addition of the phenyl unit presumably reduces this amplitude at the molecular terminus by spreading the charge distribution and hence increases T_{NFN}, see Figure 9. Indeed, we have previously suggested that this may also explain the enhanced stability of ferroelectric nematogens with additional fluorination in the terminal nitrophenyl ring [19,28]. The stability of the N_F phase therefore appears to be dictated by a combination of shape anisotropy and electronic effects. We should note that although the values for T_{NFN} are higher for the 1O(m-O*n*)PEPEBNO$_2$ series than for the **5**-*m* series, the T_{NFN}/T_{NI} ratio is lower, for example, for 1O(m-O9)PEPEBNO$_2$, the ratio is 0.744 and considerably lower than the value of 0.978 for **5**-9. This reflects the greater role played by structural anisotropy in determining T_{NI} compared to T_{NFN}.

Transitional data for the homologues of the 1O(m-O*n*)PEBNO$_2$ series (*n* = 1-2) are listed in Table 2. The conventional nematic phase is again assigned by the observation of a characteristic schlieren texture, Figure 10. An N_F phase was not observed for either compound. The N phase may be supercooled in isolated
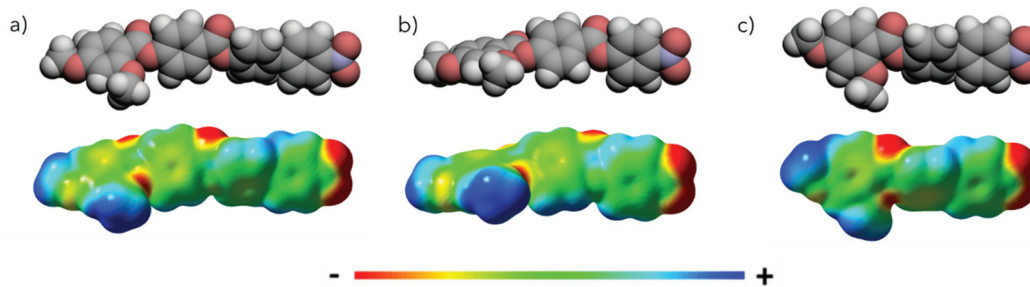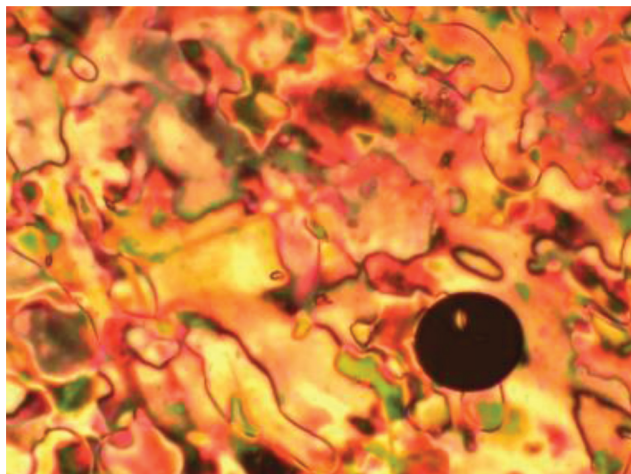

Figure 9. (Colour online) A comparison of the molecular shapes and electrostatic potential surfaces of (a) 1O(m-O1)PEPEBNO$_2$, (b) RM734 (**5**-1) and (c) 1O(m-O1)PEBNO$_2$.

Table 2. Transition temperatures and associated scaled entropy changes for the 1O(m-On)PEBNO$_2$ series.

n	T_{Cr-}/°C	T_{NI}/°C*	ΔS_{Cr-}/R	ΔS_{NI}/R
1	187	161	11.8	0.09
2	146	131	12.8	0.07

*denotes temperature obtained from DSC cooling trace.

Figure 10. (Colour online) Nematic texture of 1O(m-O2)PEBNO$_2$ at 92°C.

droplets to around room temperature, indicating a reduction in T_{NFN} by over 100°C when compared to the corresponding **5**-m homologues.

The value of T_{NI} for 1O(m-O1)PEBNO$_2$ is lower than that for **5**-1 by 27°C, but that of 1O(m-O2)PEBNO$_2$ is the same as that for **5**-2. This reflects the shape of the T_{NI} line on increasing the length of the lateral chain, and as we have seen, as the interaction strength parameter between the mesogenic units decreases, the dependence of T_{NI} becomes weaker. This is also evident if we compare the values of T_{NI} of 1O(m-On)PEBNO$_2$ and 1O(m-On)PEPEBNO$_2$. For $n = 1$, the reduction in T_{NI} is almost 200°C and this uses the lower limit of T_{NI} which as we have seen is accompanied by decomposition. This reduction falls to 160°C when comparing the values of T_{NI} for $n = 2$.

It is clear that T_{NFN} is more sensitive to the removal of the ester linkage when comparing the behaviour of 1O(m-On)PEPNO$_2$ and corresponding members of the **5**-m series, and this is in accord with earlier observations made by Mandle *et al*. [3]. For $n = 1$, the reduction in the molecular dipole moment is 1.66 D which may, at least in part, account for the reduction in T_{NFN}. Within the framework of the model proposed by Madhusudana [27], the removal of the ester linkage markedly changes the longitudinal surface charge density wave. The ester group may be thought of as an insulating fragment and divides the molecules into distinct electronic regions,

see Figure 9. Without the ester link, the electron density is more evenly distributed, resulting in the observed decrease in the stability of the N$_F$ phase.

Conclusion

The addition of the phenyl ring to **5**-1 (RM734) clearly has a significantly more pronounced effect on the value of T_{NI} than on T_{NFN}. The increase in T_{NI} of at least 172°C is wholly expected and may be attributed to the enhanced structural anisotropy and more favourable intermolecular interactions arising from the insertion of the phenyl ring. The much weaker effect on T_{NFN}, an increase of just 10°C, may reflect a change in the shape of the molecule and this now requires further study. In addition, this increase is in accord with the prediction of a molecular model that describes the molecules in the ferroelectric nematic phase as having a longitudinal surface charge density wave, and the phenyl serves to reduce this at the molecule terminus. The behaviour of T_{NI} and T_{NFN} on increasing the length of the alkyloxy chain in the 1O(m-On)PEPEBNO$_2$ and **5**-m series is essentially the same and is more pronounced for T_{NI} than for T_{NFN}. The dependence of T_{NI} may be accounted for in terms of structural anisotropy, whereas the weaker effect on T_{NFN} may be associated with the lateral chain inhibiting anti-parallel associations of the molecules. We also note, however, that these data may suggest that the stability of the N$_F$ phase is linked to the molecular shape as suggested by computer simulation studies [29]. The removal of the ester linkage between the **5**-m and 1O(m-On)PEPNO$_2$ series has a pronounced effect on the stability of the N$_F$ phase, and this appears to be consistent with the model proposed by Madhusudana [27]. We clearly have a great deal more to learn about the subtle relationship between molecular structure and the ferroelectric nematic phase.

Disclosure statement

Funding

ORCID

Ewan Cruickshank ⓘ http://orcid.org/0000-0002-4670-8405
John MD Storey ⓘ http://orcid.org/0000-0002-5261-5467
Corrie T Imrie ⓘ http://orcid.org/0000-0001-6497-5243
Rebecca Walker ⓘ http://orcid.org/0000-0001-5167-7183

References

[1] Gray GW, Kelly SM. Liquid crystals for twisted nematic display devices. J Mater Chem. 1999;9(9):2037–2050. doi: 10.1039/a902682g

[2] Born M. Über anisotrope Flüssigkeiten. Versuch einer Theorie der flüssigen Kristalle und des elektrischen Kerr-Effekts in Flüssigkeiten. Sitzungsber Preuss Akad Wiss. 1916;30:614–650.

[3] Mandle RJ, Cowling SJ, Goodby JW. Rational design of rod-like liquid crystals exhibiting two nematic phases. Chem Eur J. 2017;23(58):14554–14562. doi: 10.1002/chem.201702742

[4] Mandle RJ, Cowling SJ, Goodby JW. A nematic to nematic transformation exhibited by a rod-like liquid crystal. Phys Chem Chem Phys. 2017;19(18):11429–11435. doi: 10.1039/C7CP00456G

[5] Nishikawa H, Shiroshita K, Higuchi H, et al. A fluid liquid-crystal material with highly polar order. Adv Mater. 2017;29(43):1702354. doi: 10.1002/adma.201702354

[6] Chen X, Korblova E, Dong D, et al. First-principles experimental demonstration of ferroelectricity in a thermotropic nematic liquid crystal: polar domains and striking electro-optics. Proc Natl Acad Sci USA. 2020;117(25):14021–14031. doi: 10.1073/pnas.2002290117

[7] Folcia CL, Ortega J, Vidal R, et al. The ferroelectric nematic phase: an optimum liquid crystal candidate for nonlinear optics. Liq Cryst. 2022;49(6):899–906. doi: 10.1080/02678292.2022.2056927

[8] Brown S, Cruickshank E, Storey JMD, et al. Multiple polar and non-polar nematic phases. ChemPhyschem. 2021;22(24):2506–2510. doi: 10.1002/cphc.202100644

[9] Pociecha D, Walker R, Cruickshank E, et al. Intrinsically chiral ferronematic liquid crystals: an inversion of the helical twist sense at the chiral nematic – chiral ferronematic phase transition. J Mol Liq. 2021;361:119532. doi: 10.1016/j.molliq.2022.119532

[10] Mandle RJ. A new order of liquids: polar order in nematic liquid crystals. Soft Matter. 2022;18(27):5014–5020. doi: 10.1039/D2SM00543C

[11] Li J, Nishikawa H, Kougo J, et al. Development of ferroelectric nematic fluids with giant-ε dielectricity and nonlinear optical properties. Sci Adv. 2021;7(17):eabf5047. doi: 10.1126/sciadv.abf5047

[12] Li J, Wang Z, Deng M, et al. General phase-structure relationship in polar rod-shaped liquid crystals: importance of shape anisotropy and dipolar strength. Giant. 2022;11:100109. doi: 10.1016/j.giant.2022.100109

[13] Manabe A, Bremer M, Kraska M. Ferroelectric nematic phase at and below room temperature. Liq Cryst. 2021;48(8):1079–1086. doi: 10.1080/02678292.2021.1921867

[14] Li J, Xia R, Xu H, et al. How far can we push the rigid oligomers/polymers toward ferroelectric nematic liquid crystals? J Am Chem Soc. 2021;143(42):17857–17861. doi: 10.1021/jacs.1c09594

[15] Song Y, Li J, Xia R, et al. Development of emergent ferroelectric nematic liquid crystals with highly fluorinated and rigid mesogens. Phys Chem Chem Phys. 2022;24(19):11536–11543. doi: 10.1039/D2CP01110G

[16] Zhao X, Zhou J, Li J, et al. Spontaneous helielectric nematic liquid crystals: electric analog to helimagnets. Proc Natl Acad Sci USA. 2021;118(42):e2111101118. doi: 10.1073/pnas.2111101118

[17] Nishikawa H, Araoka F. A new class of chiral nematic phase with helical polar order. Adv Mater. 2021;33(35):2101305. doi: 10.1002/adma.202101305

[18] Mandle RJ. Supramolecular ferroelectric nematic materials. Liq Cryst. 2022;49(15):2019–2026. doi: 10.1080/02678292.2022.2145380

[19] Cruickshank E, Walker R, Storey JMD, et al. The effect of a lateral alkyloxy chain on the ferroelectric nematic phase. RSC Adv. 2022;12(45):29482–29490. doi: 10.1039/D2RA05628C

[20] Frisch MJ, Trucks GW, Schlegel HB, et al. Gaussian 09, Revision B.01. *Gaussian 09, Revision B.01.* Wallingford CT: Gaussian, Inc; 2010.

[21] Tarini M, Cignoni P, Montani C. Ambient occlusion and edge cueing to enhance real time molecular visualization. IEEE Trans Visual Comput Graphics. 2006;12(5):1237–1244. doi: 10.1109/TVCG.2006.115

[22] Donaldson T, Staesche H, Lu ZB, et al. Symmetric and non-symmetric chiral liquid crystal dimers. Liq Cryst. 2010;37(8):1097–1110. doi: 10.1080/02678292.2010.494412

[23] Yeap GY, Hng TC, Yeap SY, et al. Why do non-symmetric dimers intercalate? The synthesis and characterisation of the α-(4-benzylidene-substituted-aniline-4′-oxy)-ω-(2-methylbutyl-4′-(4″-phenyl)benzoateoxy) alkanes. Liq Cryst. 2009;36(12):1431–1441. doi: 10.1080/02678290903271504

[24] Weissflog W, Demus D. Compounds with lateral long-chain substituents — a new molecule structure concept for thermotropic liquid crystals. Cryst Res Technol. 1983;18(1):K21–K24. doi: 10.1002/crat.2170180127

[25] Weissflog W, Demus D. Thermotropic liquid crystalline compounds with lateral long-chain substituents (II).: synthesis and liquid crystalline properties of 1,4-Bis [4-substituted-benzoyloxy]-2-n-alkylbenzenes. Cryst Res Technol. 1984;19(1):55–64. doi: 10.1002/crat.2170190112

[26] Imrie CT, Taylor L. The preparation and properties of low molar mass liquid crystals possessing lateral alkyl chains. Liq Cryst. 1989;6(1):1–10. doi: 10.1080/02678298908027317

[27] Madhusudana NV. Simple molecular model for ferroelectric nematic liquid crystals exhibited by small rod-like mesogens. Phys Rev E. 2021;104(1):014704. doi: 10.1103/PhysRevE.104.014704

[28] Tufaha N, Cruickshank E, Pociecha D, et al. Molecular shape, electronic factors and the ferroelectric nematic phase. Chem A Eur J. 2023;29(28):e202300073. doi: 10.1002/chem.202300073

[29] Berardi R, Ricci M, Ricci M, et al. Ferroelectric nematic and smectic liquid crystals from tapered molecules. Chemphyschem. 2001;2(7):443–447. doi: 10.1002/1439-7641(20010716)2:7<443:AID-CPHC443>3.0.CO;2-J